Polymer(Korea), Vol. 41, No. 6, pp. 915-925 (2017)
https://doi.org/10.7317/pk.2017.41.6.915

ISSN 0379-153X(Print)
ISSN 2234-8077(Online)

성장핵을 사용한 유화중합을 통한 Poly(styrene-*co*-acrylic acid)/Polystyrene 비등방성 나노입자의 제조

Feng Zhou, Shaohui Lin, Garry L. Rempel*, and Qinmin Pan†

Green Polymer and Catalysis Technology Laboratory, College of Chemistry, Chemical Engineering and Material Science, Soochow University

*Department of Chemical Engineering, University of Waterloo

(2017년 3월 22일 접수, 2017년 5월 16일 수정, 2017년 6월 11일 채택)

Fabrication of Poly(styrene-*co*-acrylic acid)/Polystyrene Anisotropic Nanoparticles via Seeded Emulsion Polymerization

Feng Zhou, Shaohui Lin, Garry L. Rempel*, and Qinmin Pan†

Green Polymer and Catalysis Technology Laboratory, College of Chemistry, Chemical Engineering and Material Science, Soochow University, Suzhou 215123, Jiangsu Province, People's Republic of China

**Department of Chemical Engineering, University of Waterloo, Waterloo, Ontario, N2L 3G1, Canada*

(Received March 22, 2017; Revised May 16, 2017; Accepted June 11, 2017)

Abstract: Anisotropic nanoparticles have potentially various important applications, especially in 3D printing materials, binders and phase compatible agents, for which it is essential that the components and the structures are well designed and controlled. This paper investigated nanoparticles consisting of two lobes with opposite properties. As a model system, synthesis of poly(styrene-*co*-acrylic acid)/polystyrene anisotropic nanoparticles was studied and the effects of temperature, surfactant amount, inhibitors, and initiators for the involved polymerization procedures, and the swelling temperature, and swelling ratio for making the second lobe, on the morphology and size of the produced particles , were investigated. As a result, the anisotropic nanoparticles with uniform asymmetry, one lobe with hydrophilicity and the other with hydrophobicity, were successfully realized. The apparent size of the nanoparticles was below 200 nm, and the strategies for achieving various morphologies, such as snowman-like, potato-like and dumbbell-like, were established. The anisotropic nanoparticles achieved in this study are very useful in the 3D material development that is involved in our another research.

Keywords: snowman-like, anisotropic nanoparticles, 3D printing materials, hydrophilicity, hydrophobicity.

Introduction

Janus particles were named after the two-faced Roman god,[1-3] with two different chemical components or anisotropic shapes,[4] belong to the category of asymmetric particles. It has an asymmetric structure as Janus particle, confetti-like particle,[5] bicompartmental particle, dumbbell-like particle,[6] half raspberry-like particle,[7] atom-like particle, snowman-like particle,[8-11] popcorn-like particle[12] and other non-spherical composite particles.[13] Amphiphilic Janus particles have one hydrophilic and one hydrophobic face, attributing to their particles' promising properties; these can be applied to emulsion stabilization,[14,15] photonics, biosensors, drug delivery, electronics, catalyst carriers,[16] and micro reactors.[17-19] In particular, anisotropic Janus particles possess very inclusive application prospects and excellent performance, particularly being kinetically stable at the interface.[20,21] There are many innovative methods of synthesizing Janus particles, such as self-assembly of block copolymer,[13,22-24] subsequent surface modification,[25,26] seeded emulsion polymerization,[27-29] micro phase separation in confined volume,[30-33] and others.

Seeded emulsion polymerization is an effective strategy for producing non-spherical particles. Among non-spherical particles, snowman-like Janus polymer particles in shape have been extensively synthesized via seeded emulsion polymerization.[34] In a rep-

†To whom correspondence should be addressed.
E-mail: qpan@suda.edu.cn

resentative seeded emulsion polymerization, highly cross-linked spherical seeded particles are first swollen with monomer with follow-up polymerization to fabricate a variety of uniform non-spherical nanoparticles. A competition between kinetic and thermodynamic factors determined the morphology of anisotropic nanoparticles.[35-37] On the basis of these two factors, composite polymer particles with various morphologies have so far been prepared using seeded emulsion polymerization.[38,39] The kinetic and thermodynamic mechanisms are used to control phase separation[40-42] based on the seeded emulsion polymerization of non-spherical nanoparticles which have been clarified. In addition, the importance of thermodynamic and kinetic factors governing asymmetry particles were discussed in details, such as the thermodynamics of swelling, swelling kinetic and kinetic of the polymerization of asymmetrically swollen particles.

There have been a few research reports on the synthesis of anisotropic particles. For example, anisotropic particles synthesized by Sheu *et al*.[38] with characteristic sizes of 5-10 μm which settle easily under gravity. Mock *et al*.[39] synthesized anisotropic nanoparticles with average sizes from 100 to 300 nm via seeded emulsion polymerization for the purpose of obtaining uniform and small to remain colloidally stable indefinitely, but the research lacks of the monomer conversion of seed particles. Here we investigated the monomer conversion of seed particles and the synthesizing process of uniform, small and amphipathic poly(styrene-*co*-acrylic acid)-polystyrene (P(St-*co*-AA)-PS) anisotropic nanoparticles via the modified seeded emulsion polymerization. The effects of reaction temperature, swelling temperature, SDS amount, swelling ratio and different initiators on morphology, size and polydispersity index (PDI) of anisotropic nanoparticles are explored.

Experimental

Materials. Styrene (St, purity 99%) (treated by passing through basic alumina column twice to remove inhibitors and then stored in a refrigerator before being used for no longer than two weeks), acrylic acid (AA, 98%) (distilled under reduced pressure before use), sodium dodecylbenzene sulfate (SDS, AR) (used as emulsifier), and potassium peroxydisulfate (KPS, AR) (used as initiator) were obtained from the Sinopharm Chemical Reagent Co., Ltd., Shanghai. Divinyl benzene (DVB, Alfa Aesar) used as a cross-linking agent, passing through a basic alumina column twice to remove inhibitors before use. 2,2-Azobis(2-methylpropionitrile) (AIBN, 99%), and benzoyl peroxide (BPO, AR), used as an initiator were supplied by Chengdu Micxy Chemical Co., Ltd., and were purified by recrystallization before use. Ethanol (AR), methanol (AR), acrylamide (CP), methyl methacrylate (AR) and aluminum oxide were also obtained from the Sinopharm Chemical Reagent Co., Ltd., Shanghai. Sodium nitrite (AR), and hydroquinone (AR), used as aqueous phase inhibitors were obtained from the Sinopharm Chemical Reagent Co., Ltd., Shanghai. Deionized water (H_2O) used all through the experiments, was made in our lab.

Synthesis of Cross-linking Spherical Monodispersed P(St-DVB) Particles. Cross-linking spherical monodisperse poly(styrene-divinyl benzene) (P(St-DVB)) seed particles were synthesized using emulsion polymerization according to the recipes in Table 1. A 250 mL, three-necked, round-bottom flask equipped with a poly(tetrafluoroethylene) (PTFE)-coated stir bar was placed in a constant-temperature oil bath at set temperature under nitrogen atmosphere. Subsequently, H_2O and SDS were added to the reactor and allowed to reach the set reaction temperature. St and DVB were then charged into the reactor. When the contents of the flask were mixed and reached the set temperature, dissolved KPS in H_2O was added. Finally, the polymerization was allowed to take place for 24 h at the set reaction temperature under stirring of 300 rpm. The solid content and monomer conversion of the P(St-DVB) seed particles were measured gravimetrically. The solid content and monomer conversion were calculated by the following equation:

$$\text{Solid content } (\%) = \frac{W_2}{W_1} \times 100\% \quad (1)$$

and

$$\text{Monomer conversion } (\%) = \frac{W_2 - W_3}{W_4} \times 100\% \quad (2)$$

where W_1 and W_2 represent the mass of the withdrawn emulsion and the remaining solid respectively. W_3 represents the mass of SDS and the KPS. W_4 represents the mass of the theoretic mass of polymer.

The average size and size distribution of the P(St-DVB) seed particles were determined via dynamic light scattering (DLS).

Synthesis of P(St-*co*-AA) Seed Particles. AA and St were used to coat the surface of the spherical cross-linked seed particles. A 250 mL, three-necked, round-bottom flask equipped with a PTFE-coated stir bar was placed in a constant-temperature oil bath at set reaction temperature under nitrogen atmosphere. Immediately afterward, the P(St-DVB) seed emulsion and H_2O were added into the reactor and allowed to reach the oil bath temperature. St and AA were then charged into the reactor. The con-

tents of the flask were mixed and allowed to reach the set reaction temperature. Finally, dissolved KPS in H_2O was added. The polymerization was allowed to take place for 24 h at set reaction temperature under stirring of 300 rpm. The solid content and monomer conversion of the P(St-*co*-AA) seed particles were measured gravimetrically. The solid content and monomer conversion were calculated using eqs. (1) and (2). The average size and size distribution of the P(St-*co*-AA) seed particles were determined via DLS.

Seed Particle Swelling. SDS, P(St-*co*-AA) seed particles emulsion and H_2O were added to the reactor. A given amount of St was charged into the reactor and the swelling reaction was allowed to continue for 22 h under stirring of 300 rpm. The usage of SDS of 0 g, 15 mg and 40 mg and swelling ratios of 1:0.5, 1:1, 1:2 and 1:4, and swelling temperature of 25, 50 and 60 °C were explored in this study. The average size and size distribution of the swollen P(St-*co*-AA) seed particles were determined via DLS.

Second-stage Polymerization. We added hydroquinone as an aqueous phase inhibitor to prevent the formation of secondary particles in the second-stage polymerization. When the seed particles had been swollen for 22 h, the oil bath was allowed to reach set temperature. After that, a given amount of hydroquinone dissolved in 2.5 mL of H_2O was added to the swollen emulsion in the reactor and when the reactor had reached the set reaction temperature, dissolved AIBN in St was added. The second-stage polymerization was allowed to take place for 24 h at set temperature under stirring of 300 rpm. After reaction, the emulsion was placed in a centrifuge tube and centrifuged for 15 min under stirring of 10000 rpm and repeated for three times. Finally, samples were placed in a drying oven and dried for 48 h for Fourier transform infrared (FTIR) analysis. The average size and size distribution of the P(St-*co*-AA)-PS anisotropic nanoparticles were determined via DLS.

Characterization. FTIR spectra were obtained with a Nicolet iS 10 FTIR spectrometer via the pressed samples using KBr powder.

The measurements of the sizes and size distributions of the P(St-DVB) seed particles, the P(St-*co*-AA) seed particles, the swollen P(St-*co*-AA) seed particles and the P(St-*co*-AA)-PS anisotropic nanoparticles were carried out via DLS using a Zetasizer Nano S (Malvern Instruments). For sample preparation, the particle emulsion was diluted with deionized water and then was placed into a cuvette for testing. The scattering intensity was measured at a total scattering angle of 173°. The temperature of measurement was 25 °C and the reported hydrodynamic diameter was the average of the results of three DLS measurements. The data of DLS equivalent to an average of 15 independent measurements of the intensity autocorrelation obtained over a period of 30 s.

The surface morphologies of cross-linking spherical monodisperse P(St-DVB) seed particles, P(St-*co*-AA) seed particles and P(St-*co*-AA)-PS anisotropic nanoparticles were observed using a Hitachi S-4700 field scanning electron microscope (SEM) at an acceleration voltage of 15 KV. The SEM samples were prepared by drying one drop (7 μL) of the diluted dispersion of the particles emulsion on a small piece of silicon wafer and were dried at room temperature, and then sputtered with gold and directly examined without further coating of a conductive layer.

The morphologies of the P(St-*co*-AA)-PS anisotropic nanoparticles was obtained by transmission electron microscopy (TEM, FEI Tecnai G220, USA). The TEM samples were prepared by drying one drop (7 μL) of the diluted dispersion of the particles emulsion on a bronze grid and were dried at room temperature.

Results and Discussion

The whole experiment schematic illustration for the synthesis of the anisotropic nanoparticles is illustrated in Figure 1. A series of

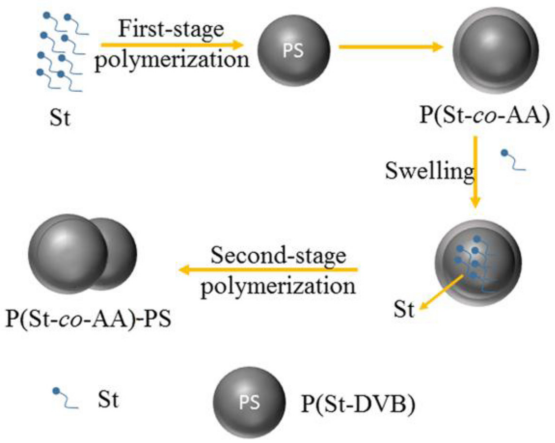

Figure 1. Schematic morphology evolution of the P(St-*co*-AA)-PS anisotropic nanoparticles.

Table 1. Polymerization Recipes for Synthesis of P(St-*co*-AA)-PS Anisotropic Nanoparticles

Entry	St (mL)	AA (mL)	SDS (g)	DVB (mL)	KPS (g)	AIBN (g)
1	15.6	-	0.126	2.6	0.390	-
2	4.5	2.1	-	-	0.099	-
3	0.44	-	0.040	-	-	-
4	0.3	-	-	-	-	0.007

Solvent: H_2O. Swelling ratio=1:2. Inhibitor: hydroquinone (2 mg).

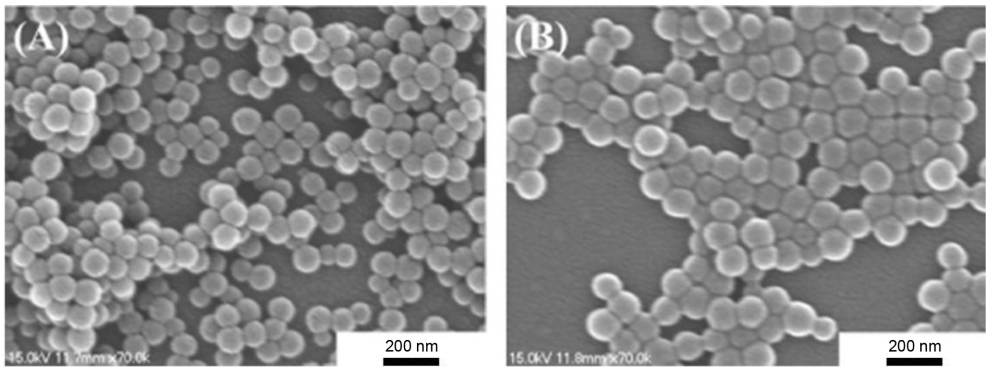

Figure 2. Morphology of (A) P(St-DVB) seed particles; (B) P(St-*co*-AA) seed particles.

Table 2. Solid Content, Average Size and Size Distributions of Particles

Entry	Solid content (%)	Average size (nm)	PDI
1	10.6	91.73	0.016
2	6.77	112.8	0.005
3	-	115.2	0.008
4	-	167.4	0.011

Solvent: H_2O. Swelling ratio=1:2. Inhibitor: hydroquinone (2 mg).

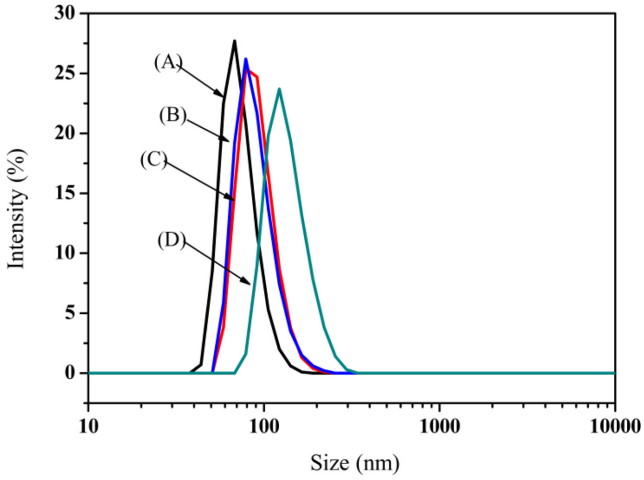

Figure 3. Size distributions of (A) P(St-DVB) seed particles; (B) P(St-*co*-AA) seed particles; (C) Swollen P(St-*co*-AA) seed particles; (D) P(St-*co*-AA)-PS anisotropic nanoparticles (solvent: H_2O; swelling ratio=1:2; inhibitor: hydroquinone (2 mg)).

experiments were carried out with different polymerization temperature, swelling temperature, SDS amount, swelling ratio, inhibitors and initiators.

Preparation of Seed Particles. Uniform monodisperse and cross-linking P(St-DVB) seed particles were prepared (Figure 2(A)) and the cross-linking P(St-DVB) seed particles had solid content of 10.6% (entry 1 in Table 2) and the monomer conversion of 99.94%. P(St-*co*-AA) seed particles (Figure 2(B)) were also fabricated with solid content of 6.77% (entry 2 in Table 2) and the monomer conversion of 98.48%.

DLS Analysis. To investigate the overall grown situation of the anisotropic nanoparticles during the polymerization, the size distributions of P(St-DVB) seed particles, P(St-*co*-AA) seed particles, swollen P(St-*co*-AA) seed particles and P(St-*co*-AA)-PS anisotropic nanoparticles were analyzed via DLS. The results are shown in Table 2 and Figure 3.

The average size of P(St-DVB) seed particles were determined to be 91.73 nm, and the PDI was 0.016 (entry 1 in Table 2). The average size of P(St-*co*-AA) seed particles were determined to be 112.8 nm, and the PDI was 0.005 (entry 2 in Table 2). The average size of swollen P(St-*co*-AA) seed particles were determined to be 115.2 nm, and the PDI was 0.008 (entry 3 in Table 2). The average size of P(St-*co*-AA)-PS anisotropic nanoparticles were determined to be 167.4 nm, and the PDI was 0.011 (entry 4 in Table 2). The size of nanoparticles was small and the PDI was very low. The results for the low PDI may be attributed to the fact that the morphology of the resulting nanoparticles was uniform (Figure 3).

Effect of the SDS Amount. Seeded emulsion polymerization process is prone to produce new colloidal particles that are not conducive to the stability and performance of the final nanoparticles.[43] The SDS amount played an important role in determining the particle size in the polymerization as it could significantly change the interfacial tension between water and micelles. In order to illustrate the role of SDS in forming the anisotropic nanoparticles, an experiment without SDS in the seed particle swelling was also conducted, for which an inconspicuous bulge

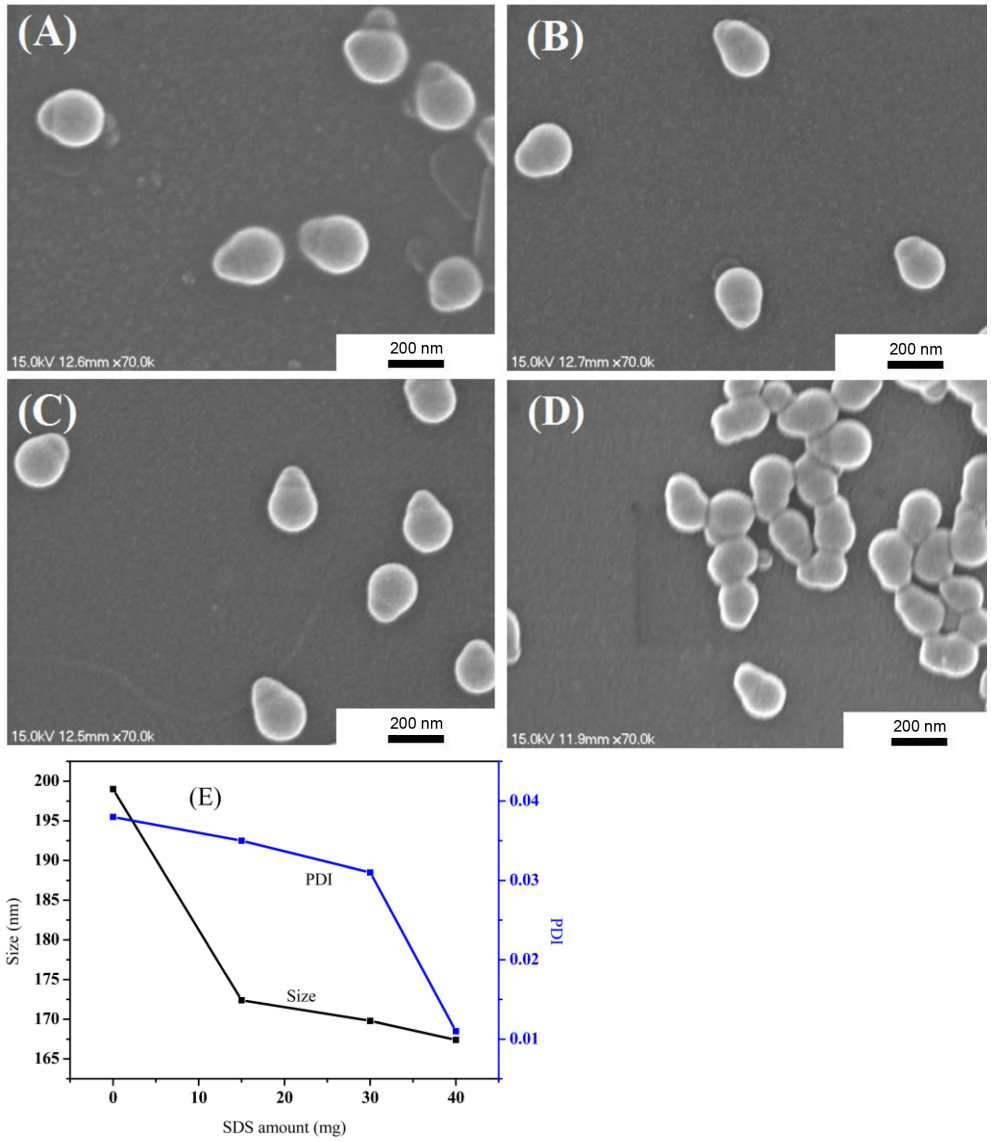

Figure 4. Morphology of the P(St-*co*-AA)-PS anisotropic nanoparticles with different amount of SDS (mg): (A) 0; (B) 15; (C) 30; (D) 40 (solvent: H_2O; swelling ratio=1:2; inhibitor: hydroquinone (2 mg); initiator: AIBN (7 mg); swelling temperature: 25 °C; second-stage polymerization temperature: 75 °C).

formed, and the SEM result is shown in Figure 4(A). With an increase in the amount of SDS, the bulge of PS became larger ((B) and (C) in Figure 4). When the amount of SDS was increased to 40 mg, the anisotropy of the P(St-*co*-AA)-PS anisotropic nanoparticles significantly increased (Figure 4(D)). The size and size distributions of P(St-*co*-AA)-PS anisotropic nanoparticles are shown in Figure 4(E). The average sizes of P(St-*co*-AA)-PS anisotropic nanoparticles decreased with increasing the SDS amount. This indicates that the SDS amount plays a key role in controlling the nanoparticle size.

Effect of Different Initiators. A method that can effectively avoid the generation of new colloidal particles is to use an oil-soluble initiator.[43] In this work, the effect of three types of initiator (AIBN, BPO and KPS) on the morphologies of P(St-*co*-AA)-PS anisotropic nanoparticles were investigated. It was observed that when the initiator was a water-soluble initiator (KPS), no lobe formed; the particle size and size distribution of the nanoparticles were close to the swollen P(St-*co*-AA) seed particles (Figure 5(C) and (D)). On the contrary, when the initiator was an oil-soluble initiator (AIBN), the anisotropy of the P(St-*co*-AA)-PS anisotropic nanoparticles was obvious, and anisotropic snowman-like nanoparticles were produced (Figure 5(B)). As the water-soluble

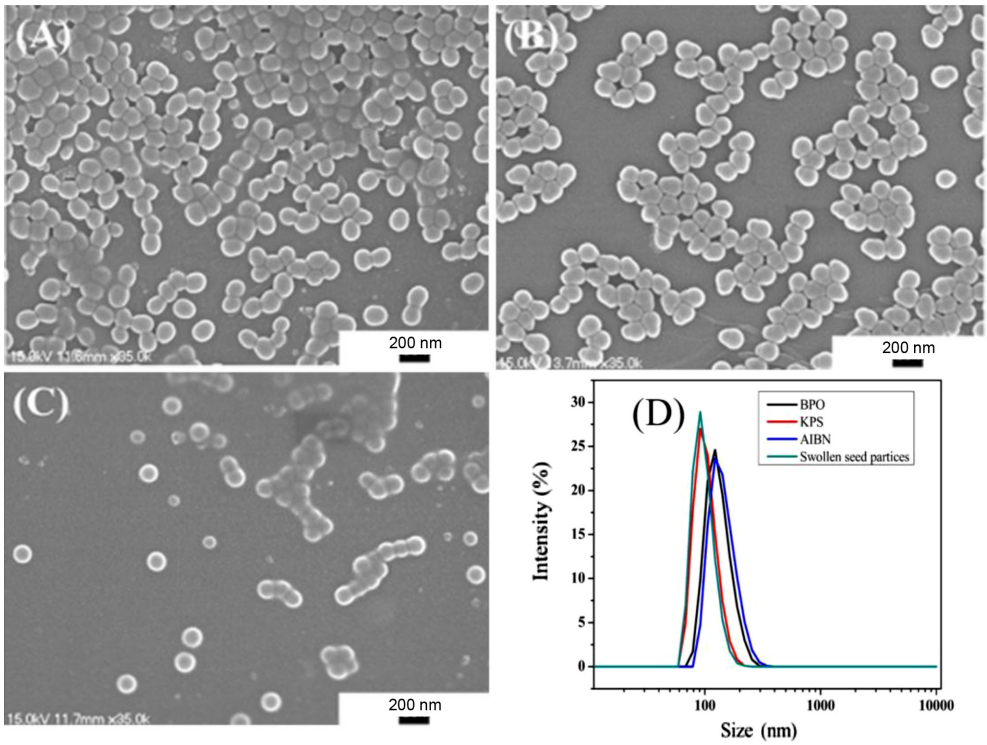

Figure 5. Morphology and size distributions of the P(St-*co*-AA)-PS anisotropic nanoparticles with different initiators: (A) BPO; (B) AIBN; (C) KPS (solvent: H_2O; swelling ratio=1:2; inhibitor: hydroquinone (2 mg); SDS amount: 40 mg; swelling temperature: 25 °C; second-stage polymerization temperature: 75 °C).

initiator prefers to stay on the surface of the micelles and an oil-soluble initiator tends to go inside the micelles, the latter has a better effect on the extrusion inside PS bulge than the former. Different morphology of nanoparticles was obtained when different type of oil-soluble initiator was used. When the initiator was BPO, a potato-like P(St-*co*-AA)-PS anisotropic nanoparticles was generated (Figure 5(A)). AIBN is insoluble in water and the decomposition rate of AIBN is slow, therefore the bulge of second-stage polymerization grows slowly. In contrast, BPO is slightly soluble in water, so the monomer dispersed in water could participate in the reaction, and the bulge of the second-stage polymerization is rapid in growth.

Effect of Different Aqueous Phase Inhibitors. The aqueous inhibitor is to suppress the monomer reaction in water. As reported in the literature, sodium nitrite[39] has been used as an aqueous phase inhibitor. In this work, two inhibitors were used to control morphology of P(St-*co*-AA)-PS anisotropic nanoparticles. No PS lobe generated when the sodium nitrite was used as an inhibitor (Figure 6(A)) although a wide range of the concentrations of sodium nitrite had been tested. Sodium nitrite is an inorganic inhibitor which suppresses monomer reaction via charge transfer with the ratio 1:1 of the chemical dosage to eliminate free radicals, so the inhibiting effect was not obvious. In contrast, when hydroquinone was used as an aqueous phase inhibitor, the size of anisotropic nanoparticles was very uniform, the morphology was snowman-like and no new colloid generated (Figure 6(B)). When the amount of hydroquinone inhibitor used was low (1 mg), some new colloid was generated (Figure 6(C)). When the hydroquinone amount was increased to 2 mg (Figure 6(B)), the effect was significantly better, although further increase in the amount led to little change (Figure 6(D)).

Effect of Swelling Temperature. The influence of swelling temperature on morphology of P(St-*co*-AA)-PS anisotropic nanoparticles is given in Figure 7. When the swelling temperature was high (60 °C), the anisotropy of P(St-*co*-AA)-PS anisotropic nanoparticles was not obvious (Figure 7(A)). With decreasing the swelling temperature to 50 °C, the resulting morphology showed one small PS bulge and the whole nanoparticles shape became irregular (Figure 7(B)). Further changed the swelling temperature to 25 °C, the PS bulge of P(St-*co*-AA)-PS anisotropic nanoparticles became larger and the morphology of P(St-*co*-AA)-PS anisotropic nanoparticles showed snowman-like (Figure 7(C)). Swelling temperature is a non-negligible factor that affects the anisotropy of anisotropic nanoparticles. When the swelling tem-

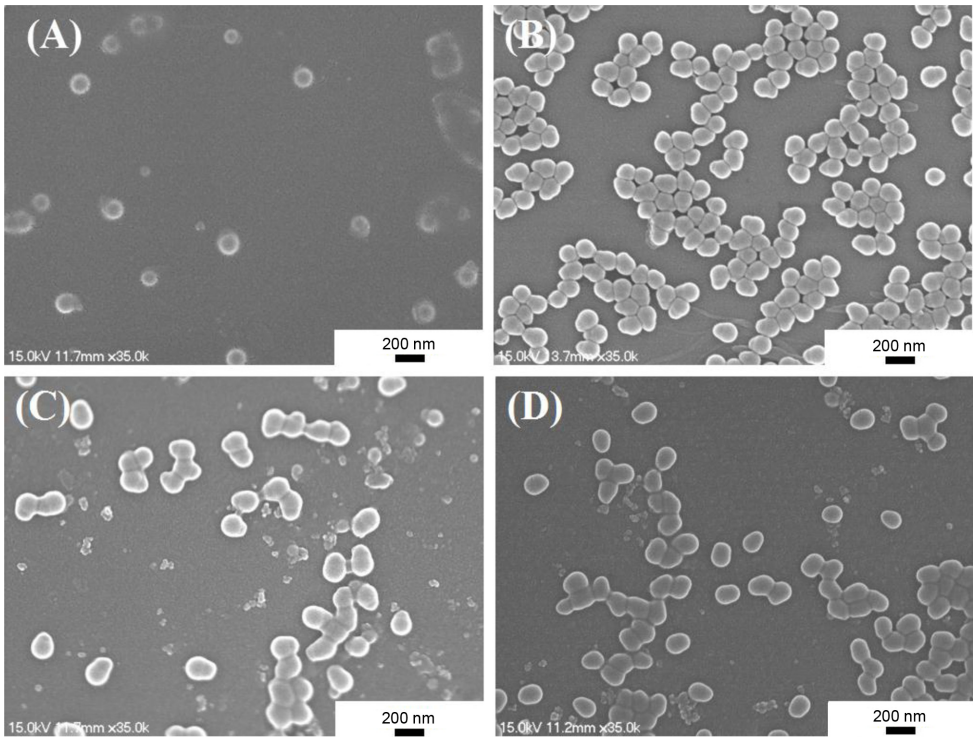

Figure 6. Morphology of the P(St-*co*-AA)-PS anisotropic nanoparticles with different types of inhibitor: (A) Sodium nitrite; (B) hydroquinone (2 mg); (C) hydroquinone (1 mg); (D) hydroquinone (4 mg) (solvent: H_2O; swelling ratio=1:2; SDS amount: 40 mg; initiator: AIBN (7 mg); swelling temperature: 25 °C; second-stage polymerization temperature: 75 °C).

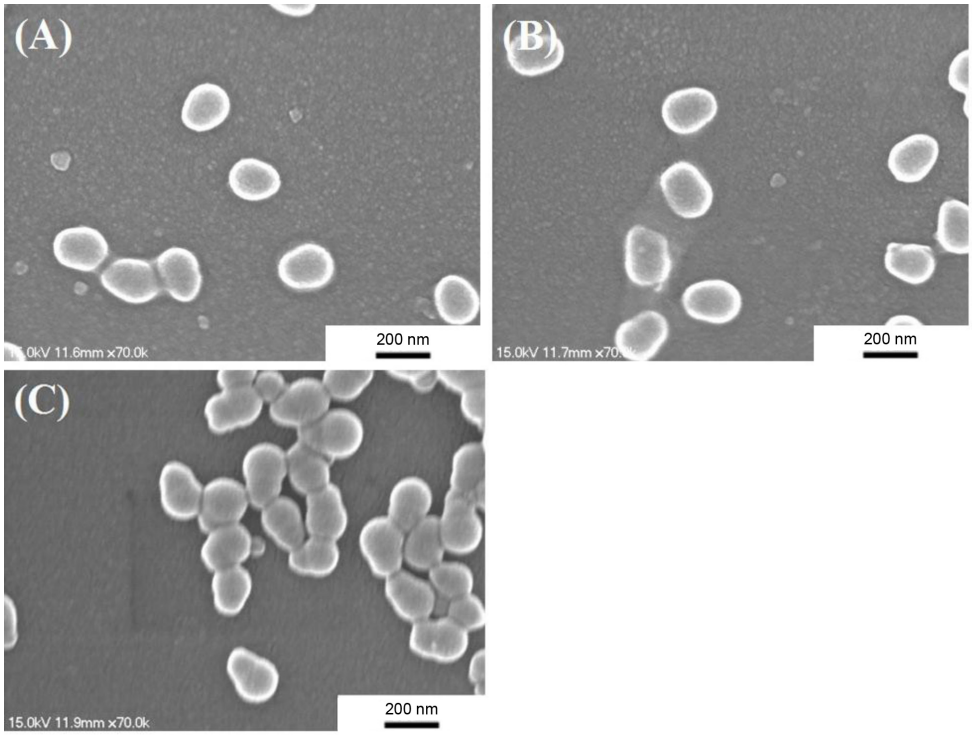

Figure 7. Morphological evolution of the P(St-*co*-AA)-PS anisotropic nanoparticles with different swelling temperature (°C): (A) 60; (B) 50; (C) 25 (solvent: H_2O; swelling ratio=1:2; inhibitor: hydroquinone (2 mg); initiator: AIBN (7 mg); SDS amount: 40 mg; second-stage polymerization temperature: 75 °C).

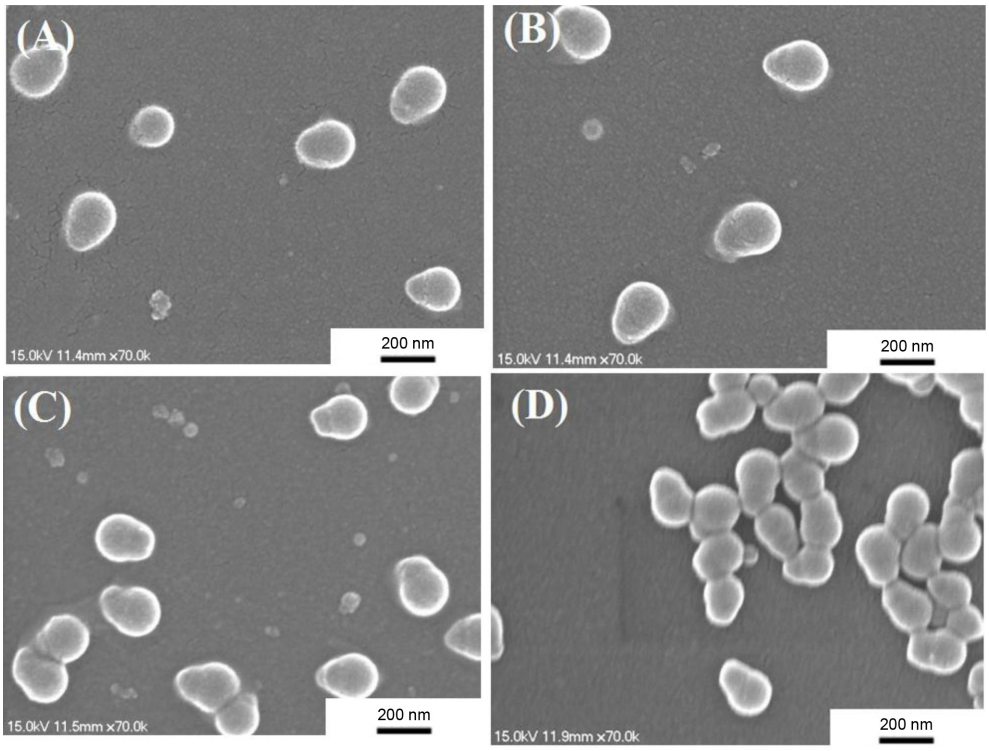

Figure 8. Morphology of the P(St-*co*-AA)-PS anisotropic nanoparticles with different reaction temperature (°C): (A) 55; (B) 60; (C) 65; (D) 75 (solvent: H_2O; swelling ratio=1:2; inhibitor: hydroquinone (2 mg); initiator: AIBN (7 mg); swelling temperature: 25 °C; SDS amount: 40 mg).

perature was increased, the diameter of the seed emulsion particles was shrunk and the space for swelling styrene monomer was reduced.

Effect of the Second-stage Polymerization Temperature. The influence of polymerization temperature on nanoparticles morphology is given in Figure 8. When the polymerization temperature was low (55, 60 °C), the anisotropy of P(St-*co*-AA)-PS anisotropic nanoparticles was not obvious ((A) and (B) in Figure 8). Further increasing the polymerization temperature to 65 °C, the anisotropy of P(St-*co*-AA)-PS anisotropic nanoparticles increased and the PS bulge was small (Figure 8(C)). We changed the polymerization temperature to 75 °C, the resulting morphology showed one big PS bulge with snowman-like morphology (Figure 8(D)). The reason for this is that the polymerization temperature mainly affects the decomposition of the initiator. When the polymerization temperature increases, the mobility of the radicals is enhanced and in turn results in higher collision rate. Beyond that, the polymerization temperature plays an important role in the phase separation. When the polymerization temperature increases, the elastic stress increases and this result in an increase in the degree of phase separation then the anisotropy of P(St-*co*-AA)-PS anisotropic nanoparticles also increase.

Effect of the Different Swelling Ratio. In previous study,[42,44] the swelling ratio of seed polymer versus swelling monomer was important to the morphology of composite particles. In this study, the effect of the swelling ratio on the morphology evolution of the P(St-*co*-AA)-PS anisotropic nanoparticles was studied. We changed swelling ratio from ratio 1:0.5 to 1:1, 1:2, and 1:4 and kept the same experimental conditions. At a small swelling ratio for example 1:0.5, the resulting morphology showed two small PS bulges (Figure 9(A)). This is because that there is not enough St to reduce the viscosity of the PS/St bulges and increase their mobility on the seed surface, therefore the newly formed PS bulges grew independently. At a swelling ratio of 1:1, most nanoparticles exhibited one PS bulge (Figure 9(B)). As seen in Figure 11(C) for seed particle swollen with a swelling ratio of 1:2, the P(St-*co*-AA)-PS anisotropic nanoparticles exhibited one small PS bulge, forming an anisotropic snowman-like particle. Further increasing the swelling ratio to 1:4, the P(St-*co*-AA)-PS anisotropic nanoparticles showed only one larger PS bulge, forming an anisotropic dumbbell-like particle (Figure 9(D)). In this situation, the St amount is liberal and it is easy for the multiple PS/St bulge to form one single bulge due to the low viscosity of the PS bulge. Beyond that, it can lower the infaust surface tension.

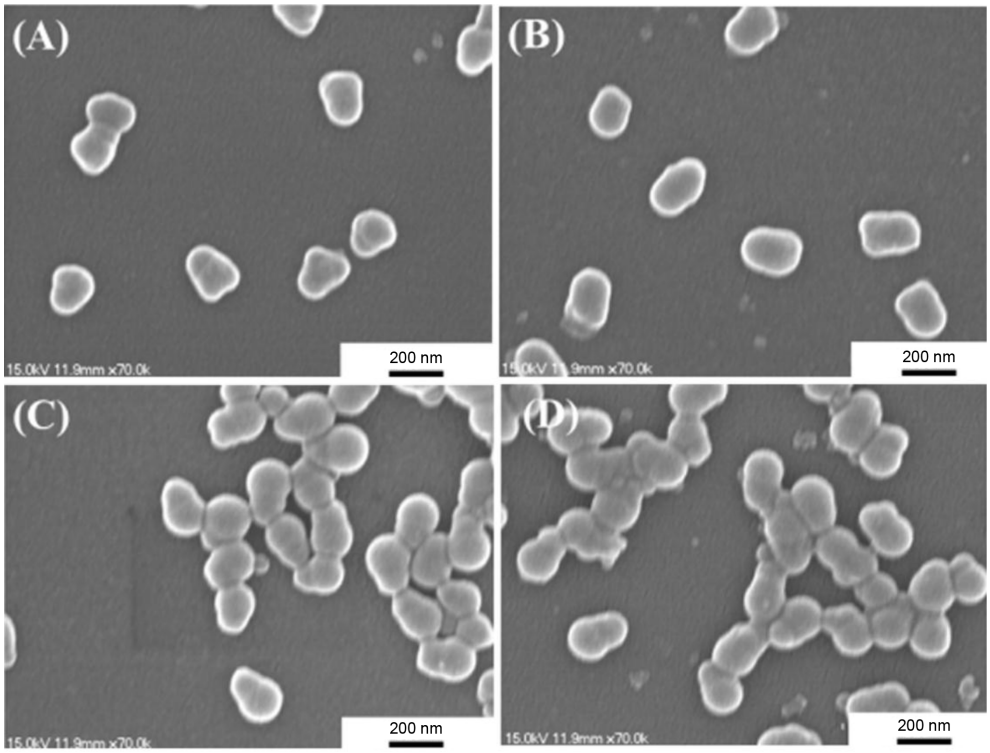

Figure 9. Morphology of the P(St-*co*-AA)-PS anisotropic nanoparticles with different swelling ratio: (A) 1:0.5; (B) 1:1; (C) 1:2; (D) 1:4 (solvent: H_2O; SDS amount: 40 mg; inhibitor: hydroquinone (2 mg); initiator: AIBN (7 mg); swelling temperature: 25 °C; second-stage polymerization temperature: 75 °C).

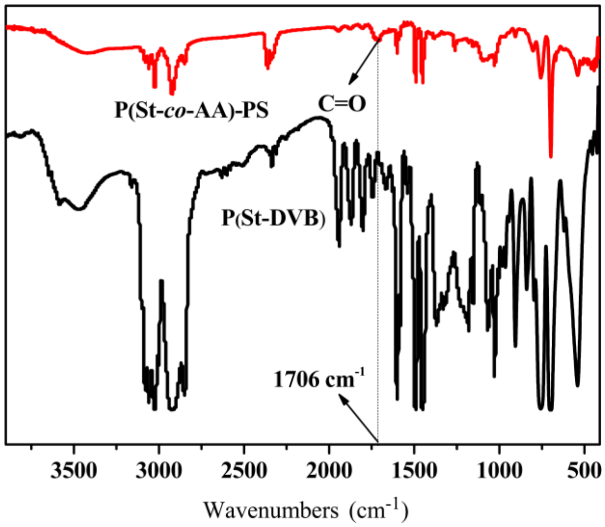

Figure 10. FTIR spectra of P(St-DVB) seed particles and P(St-*co*-AA)-PS anisotropic nanoparticles.

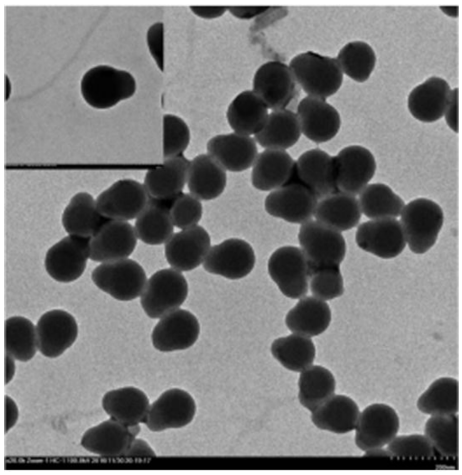

Figure 11. TEM image of P(St-*co*-AA)-PS anisotropic nanoparticles (solvent: H_2O; swelling ratio=1:2; inhibitor: hydroquinone (2 mg); AIBN (7 mg); swelling temperature: 25 °C; second-stage polymerization temperature: 75 °C).

FTIR Analysis. FTIR spectra of P(St-DVB) seeds particles and P(St-*co*-AA)-PS anisotropic nanoparticles are shown in Figure 10. The peaks at 699 and 755 cm^{-1} can be attributed to flexural vibrations (γ C-H) of the benzene ring. The bonds at 1450, 1492, 1610 cm^{-1} can be assigned to the benzene ring vibrations (C=C) in PS. The characteristic peak at 3024 cm^{-1} can be assigned to stretching vibrations (ν C-H) of unsaturated C-H groups in the benzene ring in PS. Comparing these two spectra, the absorption

peak at 1706 cm^{-1} can be attributed to stretching vibrations (ν C=O) in poly(acrylic acid) (PAA), This result indicates that acrylic acid was successfully located on the seed surface after copolymerization with styrene.

TEM Analysis. The TEM image in Figure 11 clearly shows the well-defined morphology of P(St-*co*-AA)-PS anisotropic nanoparticles and shows that P(St-*co*-AA) seed particles (the dark area) were connected by PS bulge (the light area), which confirmed that the P(St-*co*-AA)-PS anisotropic nanoparticles were formed via the phase separation caused by elastic stress.

Conclusions

We have successfully synthesized P(St-*co*-AA)-PS anisotropic nanoparticles via seeded emulsion polymerization. It was found that the types of initiator played a decisive role in determining the morphology of P(St-*co*-AA)-PS anisotropic nanoparticles. When the initiator was AIBN, the morphology of P(St-*co*-AA)-PS anisotropic nanoparticles were snowman-like or dumbbell-like; when the initiator was BPO, the morphology of P(St-*co*-AA)-PS anisotropic nanoparticles were potato-like. In addition, different types of aqueous phase inhibitor, swelling temperature, reaction temperature, SDS amount, and different initiators all had a negligible effect on controlling the shapes of the P(St-*co*-AA)-PS anisotropic nanoparticles. It is a significant discovery that controlling the phase separation is a key step in the synthesis of different shapes of anisotropic nanoparticles. When the swelling ratio increases, the anisotropy of the P(St-*co*-AA)-PS anisotropic nanoparticles increase.

Acknowledgments: Financial support from the National Natural Science Foundation of China (No. 21176163; No. 21576174), Suzhou Industrial Park, the Priority Academic Program Development of Jiangsu Higher Education Institutions and the Program of Innovative Research Team of Soochow University are gratefully acknowledged.

References

1. P. G. De Gennes, *Rev. Mod Phys*., **64**, 4 (1992).
2. Y. H. Chen, C. Y. Wang, Y. Li, and Z. Tong, *Prog. Chem.,* **21**, 7 (2009).
3. J. Lee, B. A. Yezer, D. C. Prieve, and S. H. Behrens, *Langmuir*, **32**, 3095 (2016).
4. B. Liu, J. G. Liu, F. X. Liang, Q. Wang, C. L. Zhang, X. Z. Qu, J. L. Li, D. Qiu, and Z. Z. Yang, *Macromolecules*, **45**, 5176 (2012).
5. M. Okubo, T. Fujibayashi, M. Yamada, and H. Minami, *Colloid Polym. Sci.*, **283**, 1041 (2005).
6. M. Hoffmann, Y. Lu, M. Schrinner, and M. Ballauff, *J. Phys. Chem. B*, **112**, 8 (2008).
7. H. F. Huang, and H. R. Liu, *J. Polym. Sci., Part A: Polym. Chem.,* **48**, 5198 (2010).
8. C. Tang, C. L. Zhang, J. G. Liu, X. Z. Qu, J. L. Li, and Z. Z. Yang, *Macromolecules*, **43**, 5114 (2010).
9. W. K. Kegel, D. Breed, M. Elsesser, and D. J. Pine, *Langmuir*, **22**, 2 (2006).
10. Y. D. Liu, F. F. Fang, and H. J. Choi, *Langmuir*, **26**, 6 (2010).
11. F. W. Wang, H. R. Liu, J. D. Zhang, X. T. Zhou, and X. Y. Zhang, *J. Polym. Sci., Part A: Polym. Chem.*, **50**, 4599 (2012).
12. X. Liu, M. W. Pan, J. F. Yuan, Q. Niu, X. M. Wang, and K. C. Zhang, *Rsc. Adv.*, **4**, 4163 (2014).
13. Q. Niu, M. Pan, J. Yuan, X. Liu, X. Wang, and H. Yu, *Macromol. Rapid Commun*., **34**, 1363 (2013).
14. N. Glaser, D. J. Adams, A. Boker, and G. Krausch, *Langmuir*, **22**, 3 (2006).
15. A. Walther, M. Hoffmann, and A. H. E. Müller, *Angew. Chem.*, **120**, 723 (2008).
16. H. R. Nie, C. Zhang, Y. W. Liu, and A. H. He, *Macromolecules*, **49**, 2238 (2016).
17. L. L. Zhao, L. J. Zhu, Y. Chen, Q. Wang, J. L. Li, C. L. Zhang, F. X. Liang, X. Z. Qu, and Z. Z. Yang, *Chem. Commun.,* **49**, 6161 (2013).
18. A. Kirillova, C. Schliebe, G. Stoychev, A. Jakob, H. Lang, and A. Synytska, *ACS Appl. Mater. Interfaces*, **7**, 21218 (2015).
19. T. Zentgraf, J. Valentine, N. Tapia, J. Li, and X. Zhang, *Adv. Mater.*, **22**, 2561 (2010).
20. D. Li, Y. J. He, and S. Wang, *J. Phys. Chem. C*, **113**, 3 (2009).
21. T. Tanaka, M. Okayama, H. Minami, and M. Okubo, *Langmuir*, **26**, 5 (2010).
22. A. Walther, X. Andre, M. Drechsler, V. Abetz, and A. H. E. Muller, *J. Am. Chem. Soc.*, **129**, 12 (2007).
23. R. Erhardt, A. Boker, H. Zettl, H. Kaya, W. P. Hintzen, G. Krausch, V. Abetz, and A. H. E. Mueller, *Macromolecules*, **34**, 7 (2001).
24. D. J. Kraft, W. S. Vlug, C. M. V. Kats, A. V. Blaaderen, A. Imhof, and W. K. Kegel, *J. Am. Chem. Soc.*, **131**, 5 (2009).
25. Z. F. Li, D. Lee, M. F. Rubner, and R. E. Cohen, *Macromolecules*, **38**, 4 (2005).
26. O. Cayre, V. N. Paunov, and O. D. Velev, *Chem. Commun.*, **18**, 2296 (2003).
27. J. W. Kim, R. J. Larsen, and D. A. Weitz, *J. Am. Chem. Soc.*, **128**, 4 (2006).
28. E. B. Mock and C. F. Zukosk, *Langmuir*, **26**, 13747 (2010).
29. J. G. Park, J. D. Forster, and E. R. Dufresne, *J. Am. Chem. Soc.*, **132**, 2 (2010).
30. N. Saito, Y. Kagari, and M. Okubo, *Langmuir*, **22**, 6 (2006).
31. N. Saito, R. Nakatsuru, Y. Kagari, and M. Okubo, *Langmuir*, **23**, 7 (2007).
32. N. Saito, Y. Kagari, and M. Okubo, *Langmuir*, **23**, 6 (2007).

33. T. Higuchi, A. Tajima, H. Yabu, and M. Shimomura, *Soft Matter*, **4**, 1302 (2008).
34. J. W. Kim, D. Lee, H. C. Shum, and D. A. Weitz, *Adv. Mater.*, **20**, 3239 (2008).
35. T. Fujibayashi and M. Okubo, *Langmuir*, **23**, 5 (2007).
36. M. Okubo, *Makromal. Chem., Macromol. Symp.*, **35/36**, 16 (1990).
37. Y. G. Durant, R. Carrier, and D. C. Sundberg, *Polym. React. Eng.*, **11**, 433 (2003).
38. H. R. Sheu, M. S. Elaasser, and J. W. Vanderhoff, *J. Polym. Sci., Part A: Polym. Chem.*, **28**, 22 (1990).
39. E. B. Mock, H. D. Bruyn, B. S. Hawkett, R. G. Gilbert, and C. F. Zukoski, *Langmuir*, **22**, 4037 (2006).
40. I. Cho and K. W. Lee, *J. Appl. Polym. Sci.*, **30**, 24 (1985).
41. A. T. Skjeltorp, J. Ugelstad, and T. Ellingsen, *J. Colloid Interface Sci.*, **113**, 6 (1986).
42. M. W. Pan, L. Y. Yang, B. Guan, M. S. Lu, G. J. Zhong, and L. Zhu, *Soft Matter*, **7**, 11187 (2011).
43. Q. Shao, C. G. Wang, H. Zheng, and J. M. Wang, *Polym. Bull.*, **10**, 5 (2007).
44. J. F. Yuan, L. X. Wang, L. Zhu, M. W. Pan, W. J. Wang, Y. Liu, and G. Liu, *Langmuir*, **31**, 4087 (2015).